Symmetry and Control of Spin-Scattering Processes in Two-Dimensional Transition Metal Dichalcogenides

Gilardoni, Carmem M.; Hendriks, Freddie; Wal, Caspar H. van der; Guimarães, Marcos H. D.

Published in:
Physical Review. B: Condensed Matter and Materials Physics

DOI:
10.1103/PhysRevB.103.115410

Publication date:
2021

Symmetry and control of spin-scattering processes in two-dimensional transition metal dichalcogenides

Carmem M. Gilardoni,* Freddie Hendriks, Caspar H. van der Wal, and Marcos H. D. Guimarães†
Zernike Institute for Advanced Materials, University of Groningen, NL-9747AG Groningen, The Netherlands

(Received 20 December 2020; accepted 19 February 2021; published 5 March 2021)

Transition metal dichalcogenides (TMDs) combine interesting optical and spintronic properties in an atomically thin material, where the light polarization can be used to control the spin and valley degrees of freedom for the development of novel optospintronic devices. These promising properties emerge due to their large spin-orbit coupling in combination with their crystal symmetries. Here, we provide simple symmetry arguments in a group-theory approach to unveil the symmetry-allowed spin-scattering mechanisms, and indicate how one can use these concepts towards an external control of the spin lifetime. We perform this analysis for both monolayer (inversion asymmetric) and bilayer (inversion symmetric) crystals, indicating the different mechanisms that play a role in these systems. We show that in monolayer TMDs, electrons and holes transform fundamentally differently—-leading to distinct spin-scattering processes. We find that one of the electronic states in the conduction band is partially protected by time-reversal symmetry, indicating a longer spin lifetime for that state. In bilayer and bulk TMDs, a hidden spin polarization can exist within each layer despite the presence of global inversion symmetry. We show that this feature enables control of the interlayer spin-flipping scattering processes via an out-of-plane electric field, providing a mechanism for electrical control of the spin lifetime.

DOI: 10.1103/PhysRevB.103.115410

I. INTRODUCTION

Thin layers of transition metal dichalcogenides (TMDs) offer the possibility of electrically and optically addressing spin, valley, and layer degrees of freedom of charge carriers [1–5]. This has led to increased interest in these materials for applications in novel electronic and spintronic devices [6–11]. These properties arise from the symmetries of these intrinsically two-dimensional crystals, combined with the large spin-orbit coupling imprinted on electrons by the heavy transition metal atoms in the lattice [1,4,12]. Several experimental and theoretical works explore the spin and valley lifetimes in monolayer, bilayer, and bulk TMDs, with often contrasting results. In the particular case of spin lifetime in TMDs, experimental values span over five orders of magnitude [13–18]. Group-theory-based analysis of the symmetries in this class of materials has been useful in unraveling their optical [13,19,20] and spintronic [21–23] properties, including how electrons, holes, and excitons couple to phonons and external magnetic fields, for example. This approach can be very powerful to connect and compare seemingly contrasting results, as well as giving powerful symmetry-based predictions for the design of future experiments. However, the literature still lacks a pedagogical derivation of the mechanisms leading to spin scattering in monolayer and, particularly, bilayer TMDs based solely on the symmetry of these materials. Moreover, a careful analysis and understanding of the impact of crystal symmetries on the spintronic properties of these materials can lead to better device engineering, which exploits symmetry breaking for active control over the spin information.

Here, we apply group-theoretical considerations to obtain the symmetry of the electronic wave functions at the edges of the bands in these semiconductors, for both monolayer and bilayer systems. In order to do this, we use double groups to unravel the transformation properties of the Bloch wave functions, including spin at the high-symmetry points in the Brillouin zone (BZ), in the absence of external fields. Based on these results, we derive the first-order selection rules for spin-scattering processes in a single-particle picture. This allows us to determine how electron and hole spins couple to phonons and external fields, and which mechanisms dominate spin-flipping processes at low temperatures. Based on these results, we find that electrons and holes in these materials transform differently. In particular, a combination of rotational symmetry and strong spin-orbit coupling (SOC) strongly suppresses low-temperature spin-scattering mechanisms for conduction-band electrons in monolayer TMDs. For bilayer (and few-layer) systems where individual layers are partially decoupled, we find that an electric field enhances interlayer spin-scattering processes, enabling electrical control of an optically created spin polarization. Despite being based on several approximations, the group-theoretical framework developed here allows us to intuitively understand various spin properties of this class of materials in a straightforward manner and in line with recent experimental results.

This paper is organized as follows: in Sec. II, we focus on monolayer TMDs and their symmetries. We obtain the transformation properties of the Bloch wave functions, including

*c.maia.gilardoni@rug.nl
†m.h.guimaraes@rug.nl

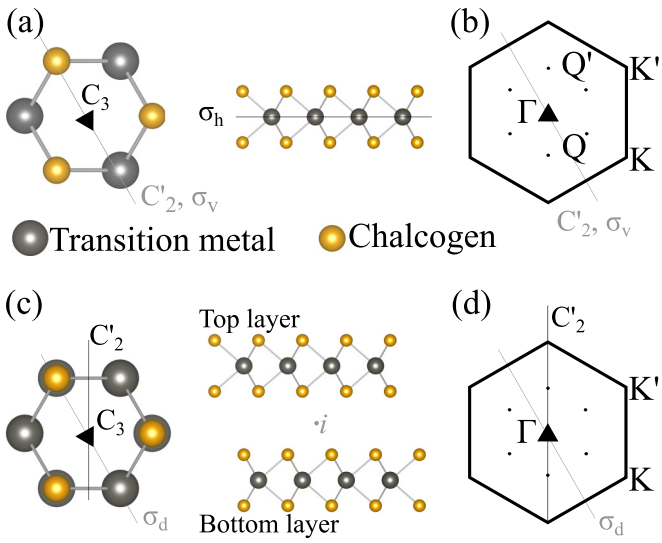

FIG. 1. Symmetry of the group of the wave vector at the K and K' points. Lattice structure in real and reciprocal space for (a), (b) monolayer and (c), (d) bilayer TMDs. The symmetry of the full crystal (that is, the symmetry at the Γ point in the BZ) is D_{3h} for the monolayer and D_{3d} for the bilayer, for which the symmetry operations are explicitly shown. Operations that, although present in the Γ point of the BZ, are absent in the K and K' points (b), (d) are shown in light gray. The absence of these symmetry operations at the K and K' points reduces the symmetry at these points to the point groups C_{3h} for monolayers and D_3 for bilayers.

spin at the high-symmetry points of the BZ. Based on the symmetries of these wave functions, we derive which perturbations (electromagnetic fields and lattice phonon modes) can couple eigenstates with opposite spin, which allows us to determine the processes most likely to lead to spin flips at low temperatures. In Sec. III, we repeat this analysis for bilayer TMDs. Finally, in Sec. IV, we summarize the main conclusions and elaborate on the impact of our findings to past and future experiments in the field.

II. MONOLAYER TMDs

A. Symmetries of the spatial eigenstates

In order to derive the spin-scattering selection rules at the edges of the bands, one must first obtain the symmetry properties of the eigenstates at the K and K' points of the BZ. These properties are determined by the point group describing the crystallographic symmetry at these points, the orbital character of the wave functions, and the spin of the charge carriers in these states [12]. In this way, we can classify the electronic eigenstates at the band edges in these materials by their transformation properties, which are summarized by the irreducible representation (IR) of the suitable point group.

A TMD monolayer (ML) is composed of transition metal and chalcogen atoms, arranged in a hexagonal lattice. Although the coordination between these atoms can vary, the most widely studied TMD polytypes (2H types) have a transition metal atom bound to six chalcogen atoms in a trigonal prismatic geometry [Fig. 1(a)], giving rise to the crystallographic point group D_{3h}. However, the edges of the valence and conduction bands in ML TMDs are located at the K and K' points of the BZ, where not all symmetries of the lattice are preserved. Here, only the threefold rotational symmetry axis (C_3), the horizontal mirror plane (σ_h), and their combinations are valid symmetry operations, such that the wave functions at the K and K' points of the BZ transform according to the point group C_{3h} [12,19,21]. Figure 1(a) shows the symmetry operations at the K and K' points in black, and the additional symmetry operations in the Γ point in gray.

Ab initio calculations and tight-binding models of these materials show that the orbital character of the electronic wave functions at the K and K' points are largely composed of the d orbitals of the transition metal atoms [24–26]. The valence-band wave functions are composed predominantly of linear combinations of $d_{x^2-y^2}$ and d_{xy} orbitals, while the conduction-band wave functions are composed predominantly of the d_{z^2} orbital localized at the transition metal atoms. Based on this, we can visualize the transformation properties of the wave functions at the edges of the valence and conduction bands [Fig. 2(a)]. To obtain the symmetry-adapted eigenstates delocalized through the lattice, one takes the wave function centered at a single transition metal atomic site and performs on it all symmetry-group operations. Due to the nonzero momentum at the K and K' points, a symmetry operation that changes the atomic site of the orbital incurs an additional phase factor ($e^{\pm i2\pi/3}$). The total (symmetry-adapted) eigenstate is found by summing the results of all symmetry operations, including these phase factors [Fig. 2(b)]. Additionally, a phase factor must also be considered when the atomic orbital itself is rotated, which depends on its azimuthal phase [represented by the color in Figs. 2(a) and 2(b)]. The conduction-band states at the K (K') points are formed mainly by d_{z^2} orbitals, which do not have any azimuthal phase. For these eigenstates, the only phase contribution when combining orbitals in different lattice sites arises from the winding of the k vectors, leading to an out-of-site phase winding. Thus, the conduction-band wave functions at the K (K') points transform according to the E'_+ (E'_-) IR of the point group C_{3h}. In contrast, valence-band states are formed predominantly by linear combinations of the $d_{x^2-y^2}$ and d_{xy} orbitals. These states are combined either as $(d_{x^2-y^2} + id_{xy})$ or as $(d_{x^2-y^2} - id_{xy})$, such that they have an orbital angular momentumlike phase winding within the atomic orbital [small arrows in Fig. 2(b), bottom]. This is in contrast with the out-of-site phase winding of the conduction-band states, which gives implications to the spin-orbit coupling as explained in the following paragraphs. These linear combinations gain a phase factor of $e^{i2\pi/3}$ or $e^{-i2\pi/3}$, respectively, when subject to a threefold rotation. Combined with the phase acquired due to the winding of the k vector, this gives rise to a wave function composed of a fully in-phase linear combination of orbitals in adjacent lattice sites. In symmetry terms, these valence-band wave functions transform as the A' IR of the C_{3h} point group. We note that to describe the full microscopic character of the valence-band (VB) and conduction-band (CB) wave functions, we should also consider contributions from the chalcogen orbitals. We chose not to do this in our approximation since it will not impact the symmetry character of the wave functions, although it will be relevant for quantitatively estimating matrix elements and energy splittings.

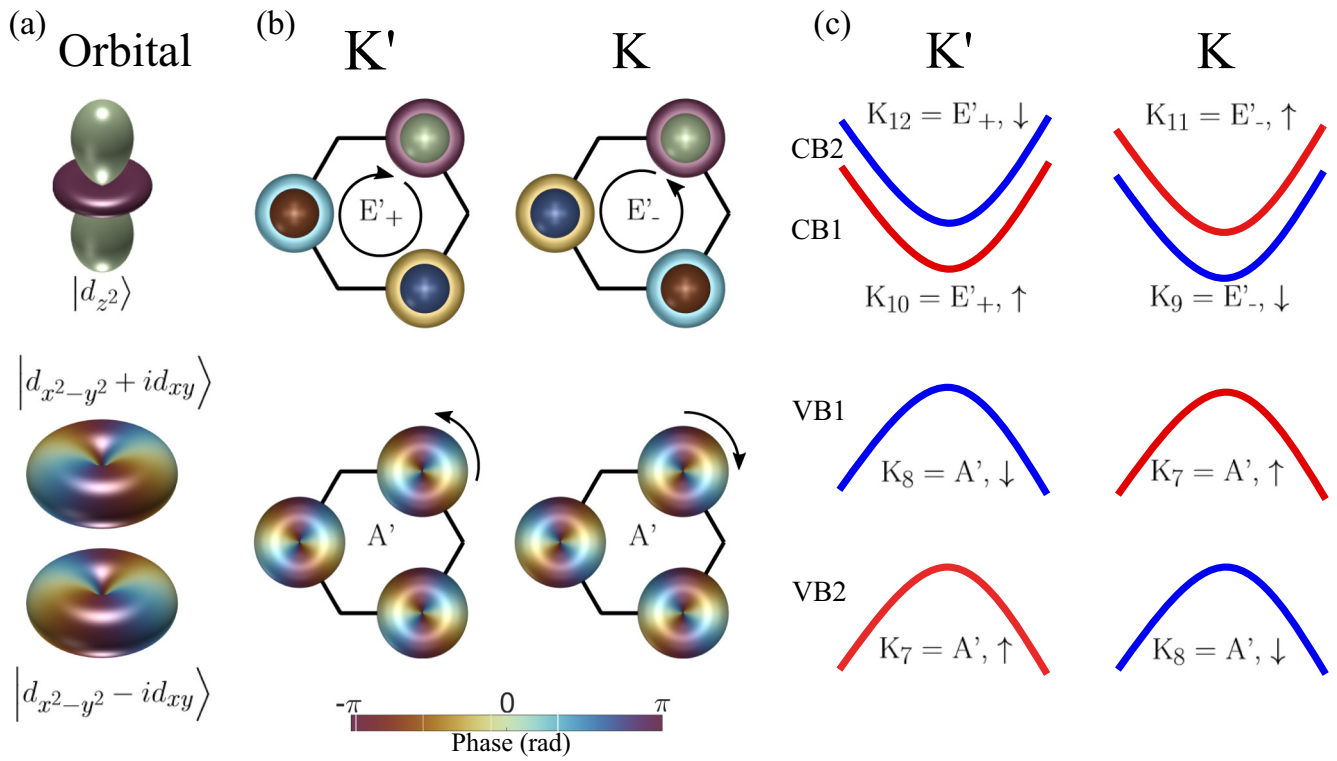

FIG. 2. Electronic wave functions at the K and K' points. (a) We can obtain the symmetry of the wave functions at the K and K' points by applying the symmetry operations of the system to the atomic d orbitals localized around the TM atoms. In a monolayer, the electronic wave function at the edge of the conduction band is mainly composed of TM $|d_{z^2}\rangle$ atomic orbitals, which has constant azimuthal phase. [In (a) and (b), the magnitude of the wave function in real space is indicated by the surface, whereas the color corresponds to the azimuthal phase according to the scale in the color bar]. (b) Top: When also considering the phase acquired due to translation, the electronic wave function at the K (K') point transforms as the E'_+ (E'_-). Bottom: In the valence band, the electronic wave function at the K and K' points is mostly composed of TM $|d_{x^2-y^2}\rangle$ and $|d_{xy}\rangle$ atomic orbitals, which can be combined into the spherical harmonics with $L = 2, m_l = \pm 2$. The phases acquired due to rotation of the spherical harmonics and translation cancel out, to give a final state that transforms as A' in both K and K' points. (c) When also considering the properties of the spin under rotation, we obtain the symmetry of the spin-orbit split wave functions in the valence and conduction bands by multiplying the IRs of (b) with the irreducible representations associated with spin up and down (K_7 and K_8, respectively). Hybridization with other orbitals will not change the particular symmetry of the wave functions.

B. Symmetries of the spin-orbit coupled eigenstates

Finally, we must also take into account the electron and hole spin when obtaining the symmetry of the wave functions. This can be done by the use of a double group approach [27]. The symmetry of the spin-orbit coupled wave function can be obtained by taking the product $\Gamma_{\text{spatial}} \times \Gamma_{\text{spin}}$, where Γ_{spatial} is the IR describing the transformation properties of the spatial wave function, and Γ_{spin} describes the transformation properties of a spin 1/2. A free spin up transforms as the IR ${}^2\bar{E}_3$ of the double group $\bar{C}_{3h}$, whereas a free spin down (its time-reversal conjugate) transforms as IR ${}^1\bar{E}_3$. Note here that a rotation by 2π adds a phase of -1 on the spin-1/2 state. Based on this, we can obtain the symmetry properties of the spin-resolved wave functions at the edges of the valence and conduction bands at the K and K' points, shown in Fig. 2(c).

All IRs of the double group $\bar{C}_{3h}$ are nondegenerate. This means that as has been widely established [1,4,15,21,28], spin and valley degrees of freedom are coupled in both valence and conduction bands, giving rise to nondegenerate spin-polarized states. In this way, spin-up and spin-down states in both valence and conduction bands are split by a spin-orbit energy splitting. The sign and magnitude of this spin-orbit energy splitting depends on the material properties and cannot be obtained from this purely group-theoretical approach. Despite the differences between the various TMDs, however, this spin-orbit splitting is, in general, an order of magnitude larger in the valence band (usually hundreds of meVs) than in the conduction band (usually tens of meVs) [25]. We can understand this order-of-magnitude difference based on the considerations above. For wave functions in the valence band, the orbital angular momentum arises from the atomic orbitals themselves, which show an azimuthal phase winding around the transition metal nuclei [as indicated by the color and small arrows in the lower panel of Fig. 2(b)]. This is clear if we rewrite the linear combinations of $d_{x^2-y^2}$ and d_{xy} in terms of spherical harmonics. This large and well-defined orbital angular momentum, localized around the nuclei, gives rise to a large spin-orbit coupling energy. In contrast, in the conduction-band states, there is an intercellular angular momentum arising from phase winding between different lattice sites [29,30]. In addition to that, we note that hybridization with p orbitals also plays a role on the SOC magnitude in the valence band, which is not explicitly considered here.

We note that the ordering of states as depicted in Fig. 2(c) is valid for tungsten-based TMDs; for molybdenum-based TMDs, the order in energy of CB1 and CB2 is reversed [25]. Nonetheless, the group-theoretical considerations presented here do not depend on the energy ordering of states and remains valid for both cases. In what follows, we will focus on the symmetry-restricted scattering processes for charge carriers in the top subband of the valence band (VB1, transforming as $K_{7,8}$), and in the two subbands of the conduction band (CB1,2 transforming as K_{9-12}). We disregard the impact of states belonging to the lower subband of the valence band (VB2) due to the large SOC energy splitting of hundreds of meV. Nonetheless, since these states also transform as $K_{7,8}$, this does not incur any loss of generality since all scattering mechanisms obtained involving VB1 would be the same as the ones involving VB2.

C. Selection rules

Given the symmetries of the various wave functions at the band edges, we can obtain the selection rules governing the spin-flipping scattering processes in these materials at low temperatures. According to Fermi's golden rule, a charge carrier in a state $|\psi_i\rangle$ can only scatter into a state $|\psi_f\rangle$ due to a perturbation H' if the matrix element $\langle\psi_i|H'|\psi_f\rangle$ is nonzero. In symmetry terms, this means that the scattering is only possible when the product of IRs, $\Gamma_i^* \otimes \Gamma_{H'} \otimes \Gamma_f$, contains the fully symmetric representation, i.e., A'. Here, $\Gamma_{i(f)}$ indicates the IR of the initial (final) states, whereas $\Gamma_{H'}$ indicates the IR of the operator responsible for the perturbation. Additionally, we note that phonons interact with electrons via the electric fields created by atomic displacements. In this way, we can also consider selection rules for phonon-driven transitions by looking at the symmetries of these electric fields. Using this, we can determine which spin-flip scattering processes a perturbation can cause, just by looking at the symmetry of the perturbation. In the following, we focus on the spin-flipping mechanisms at the K and K' points of the BZ. In the Supplemental Material [31], we provide the product tables and also the analysis for spin-conserving transitions and scattering into other points of the BZ.

These selection rules (for spin-flipping transitions only) are presented comprehensively for a monolayer TMD in Figs. 3(a) and 3(b). Only operators transforming as A'' and E'' can generate spin-flipping transitions in ML TMDs. In Fig. 3, dashed arrows indicate optical transitions. These transitions can be actively driven by electromagnetic fields in the optical spectrum or arise from radiative electron-hole recombination. Comparison with Table I shows that spin-flipping direct optical transitions are associated with the absorption or emission of electric fields polarized perpendicular to the plane of the TMD layer. The creation of these "dark" excitons via this process has been demonstrated by illuminating the TMD monolayer with a parallel beam polarized out of plane [32]. Additionally, it has been shown that an external in-plane magnetic field can also "brighten" these transitions, which can be understood as a mixing between the two states belonging to CB1 and CB2 [19,33].

Besides this spin-flipping optical transition, only operators transforming as E'' of the C_{3h} point group can give rise to spin-scattering transitions between electronic states at the various band edges in ML TMDs. These operators correspond to magnetic fields in the plane of the ML, out-of-plane phonons at the K point of the acoustic phonon band, and optical phonons at both the Γ and K points, for example (see Table II). These phonon modes have energies of the order of hundreds of meVs [12,34]. Thus, they will be very weakly populated at cryogenic

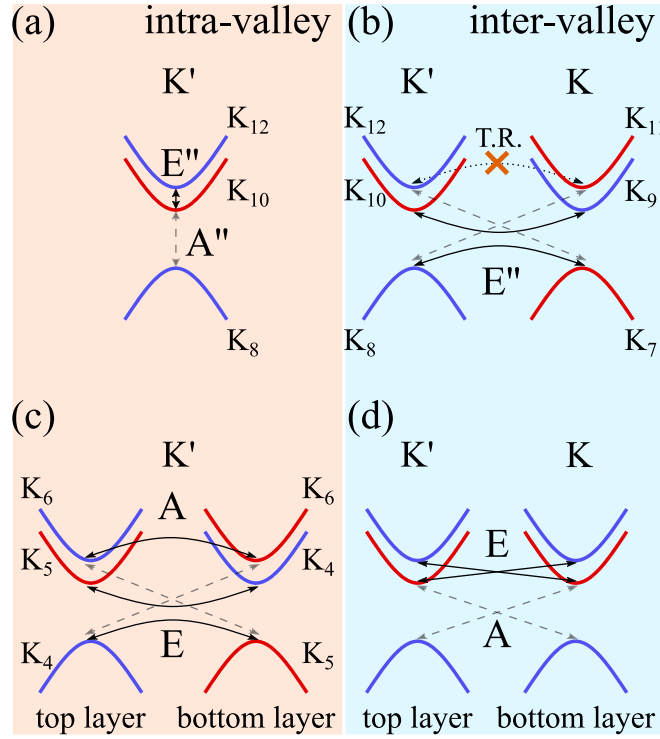

FIG. 3. Symmetries of spin-flipping scattering mechanisms in ML and bilayer (BL) TMDs. In monolayer TMDs, only operators transforming as the E'' and A'' IR of the C_{3h} group can lead to either (a) intravalley or (b) intervalley spin-flipping scattering processes. In these materials, states transforming as $K_{11,12}$ distinguish themselves since energy-conserving scattering between these states is forbidden by time-reversal symmetry (see text). (c), (d) In contrast, in bilayer TMDs, additional interlayer spin-flipping scattering processes arise, which can couple to external fields transforming as either the A or E IR of the C_3 point group. Here, optical transitions are denoted by a dashed line.

TABLE I. Symmetries of operators and phonon modes according to the group of the wave vector at the K and K' points for monolayer TMDs. LA (LO), TA (TO), and ZA (ZO) correspond to longitudinal, transverse, and out-of-plane acoustic (optical) phonon modes, respectively, [12,34].

		Acoustic phonons		Optical phonons	
C_{3h} IR	EM fields	$\Gamma, \mathbf{q}=0$	$K, \mathbf{q}\neq 0$	$\Gamma, \mathbf{q}=0$	$K, \mathbf{q}\neq 0$
A'	$\mathbf{B}_\perp$		LA/TA	ZO	LO/TO
A''	$\mathbf{E}_\perp$	ZA		ZO	LO/TO
E'	$\mathbf{E}_\parallel$	LA/TA	LA/TA	LO/TO	LO/TO
E''	$\mathbf{B}_\parallel$		ZA	LO/TO	LO/TO/ZO

temperatures, leading to a suppression of phonon-related upwards scattering processes. We note that this is also valid for Mo-based TMDs, despite their small SOC splitting between CB1 and CB2. In this case, even though the bands are close in energy, hot phonons are required to drive the transition. In contrast, downwards scattering processes ($K_{12} \rightarrow K_{10}$) can happen via the emission of a phonon even at low temperatures. This process should be distinct for molybdenum- and tungsten-based TMDs since the order of the two bands are interchanged, while the optical transition used to generate a spin-valley population ($K_8 \rightarrow K_{12}$) is the same. Our analysis then indicates that at low temperatures, the spin lifetime for electrons in molybdenum-based TMDs should, in principle, be longer than when compared to tungsten-based ones. This can be used to understand the long spin lifetimes recently reported for $MoSe_2$, which persist up to room temperature [17]. We do note that in-plane magnetic fields will be more effective in driving intravalley spin flips of spins in the CB of Mo-based TMDs, when compared to W-based TMDs. This is because the energy splitting between CB1 and CB2 is much smaller in the former, and thus easier to overcome by Zeeman-like energy terms.

When considering intervalley scattering processes, we must note that additional selection rules arise due to time-reversal symmetry and Kramer's theorem (see Supplemental Material [31]). Kramer's theorem states that if time-reversal symmetry is preserved, wave functions connected by conjugation have the same energy, that is, a spin-up in a K valley and the corresponding spin-down in the K' valley have the same energy. This implies that energy-conserving spin-flipping scattering processes between the K and K' valleys (intervalley) can only arise due to perturbations that break time-reversal symmetry (see Supplemental Material [31]). Transitions between time-conjugate pairs transforming as $K_7 \leftrightarrow K_8$ and $K_9 \leftrightarrow K_{10}$ can arise due to perturbations transforming as E''. Since in-plane magnetic fields and K phonons transforming as E'' break time-reversal symmetry, these scattering processes are thus also fully allowed by time-reversal (TR) symmetry [35]. This is in line with the experimental observations that identify out-of-plane K phonons as the main sources of hole spin-valley depolarization in both W- and Mo-based TMDs [2,3,15]. In contrast, transitions between states transforming as $K_{11} \leftrightarrow K_{12}$ are allowed—considering only spatial symmetry—when these states interact with external fields transforming as A''. Out-of-plane electric fields and Γ-point phonons (see Table I) preserve time-reversal symmetry, such that they cannot drive these transitions. In contrast, chiral K phonons in the optical phonon bands [35] do break time-reversal symmetry and could drive these transitions. Nonetheless, these are high-energy phonon modes which are not populated at low temperatures.

The results of the last paragraph point to a fundamental asymmetry in the behavior of electron and hole spin-scattering processes in these materials and are in line with the existing literature. For example, the selection rules obtained above provide an intuitive interpretation of the theoretical and experimental results, showing that in Mo-based TMDs, phonon-related spin decay affects holes in VB1 much more efficiently than electrons in CB1 at low temperatures [17] (note that in Mo-based TMDs, states in CB1 transform as $K_{11,12}$). Additionally, despite the seemingly simplistic single-particle picture presented here, these results also provide an explanation for the recently observed asymmetry between bright and dark excitons concerning direct to indirect exciton scattering in W-based TMDs [36], where indirect excitons are composed of an electron and a hole in opposite valleys.

Finally, the selection rules derived in this section imply that in monolayer TMDs, spin scattering is relatively robust with respect to the presence of noisy electric fields, such as randomly distributed Coulomb scatterers and local strain. Only out-of-plane electric fields can cause spin-flipping scattering transitions; however, these transitions are either in the optical range—such that they must be actively driven or arise from electron-hole radiative recombination—or forbidden by the requirements of Kramer's theorem. Thus, in the low-energy scattering regime, local (due to the electrostatic environment, strain of the material, substrate effects, etc.) or global electric fields will have limited influence on the prevalence of various spin-scattering processes. This also means that spin-scattering rates in ML TMDs should not be greatly influenced by the symmetry breaking created by a particular substrate. In contrast, in-plane magnetic fields, either extrinsic or intrinsic to the sample due to spin-active defects or nuclear spins, can cause both intra- and intervalley spin flips. On the one hand, these results indicate that the spin lifetimes in ML devices can be enhanced by ensuring a low concentration of deep-level spin-active lattice defects. On the other hand, they also indicate that control over the spin polarization in these materials relies on externally applying magnetic fields, which is a slow and practically challenging process.

III. BILAYER TMDs

A. Symmetries and eigenstates

Figures 1(c) and 1(d) show the symmetries of bilayer 2H-TMDs in both real and reciprocal space (symmetry operations valid at the Γ point but absent at the K and K' points are shown in gray). When compared to monolayer crystals, bilayer stacks of 2H-TMDs have some notable symmetry changes (see Fig. 1) [12]. In particular, bilayers lack a horizontal mirror plane, but do have an inversion point which brings the top layer into the bottom one. The presence of inversion symmetry means that if we consider the entire stack, spin-valley coupling is not allowed to exist—electronic eigenstates at the K and K' points are spin degenerate. However, a local spin polarization of the bands may arise when inversion symmetry is present at a global scale, but is locally broken [37]. Since interlayer coupling is small compared to the other intrinsic energy scales in 2H-TMDs [28,38], this local spin polarization arises within each ML making up the multilayer stacks, giving rise to a spin-valley-layer coupling [37,38], which has been experimentally observed [39–42]. These results are evidence that the layers are partially decoupled, such that the system can be approximately described by a stack of two distinguishable monolayers whose crystallographic symmetry corresponds to point group C_{3v}. The horizontal mirror plane and twofold axes in Figs. 1(a) and 1(b) are no longer valid symmetry operations, since the top and bottom environments of each layer differ. At the K and K' points, this symmetry is reduced to C_3, such that

TABLE II. Symmetries of operators and phonon modes according to the group of the wave vector at the K and K' points for bilayer TMDs.

		Acoustic phonons		Optical phonons	
C_3 IR	EM fields	$\Gamma, \mathbf{q}=0$	$K, \mathbf{q}\neq 0$	$\Gamma, \mathbf{q}=0$	$K, \mathbf{q}\neq 0$
A	$\mathbf{E}_\perp, \mathbf{B}_\perp$	ZA	LA/TA	ZO	LO/TO
E	$\mathbf{E}_\parallel, \mathbf{B}_\parallel$	LA/TA	LA/TA/ZA	LO/TO	LO/TO/ZO

the electronic eigenstates at the edges of the bands in each layer transform as IRs of the double group $\overline{C}_3$. Since the bottom layer is inverted with respect to the top layer, the direction of the phase winding of the eigenstates at the K and K' points of the BZ happens in opposite directions for each of the layers. This means that at a given energy and at a given point of the BZ, eigenstates in different layers will have opposite orbital and spin angular momentum. This results in a alternating spin-valley ordering according to the layer number, i.e., the top of the valence band of the valley K of one layer has the same spin (and symmetry) as the top of the valence band of the opposite valley (K') of the adjacent layer. The resulting band structure, with the respective symmetries of each of the eigenstates, can be found in the Supplemental Material [31].

B. Selection rules

Treating the layers as distinguishable does not mean that they are fully independent. This means that the additional layer degree of freedom of TMD bilayers allows for additional interlayer scattering processes. The intralayer scattering processes are the same as the ones treated in detail in Sec. II and will not be repeated here. The selection rules for the interlayer processes can be obtained in the same manner as before, now considering eigenstates and operators transforming as IRs of the double group $\overline{C}_3$. These additional spin-flipping scattering pathways are shown in Figs. 3(c) and 3(d).

Notably, the situation is drastically different for spins that are protected from energy-conserving spin-flipping scattering processes in a ML due to TR symmetry. These states transform as $K_{11,12}$ in a ML, and as K_6 in the bilayer. These charge carriers can now flip their spin by going from one layer into the other after interacting with an operator transforming as the A IR of the point group C_3. This is because, for states in the K valley for example, a spin-up in the top layer and a spin-down in the bottom layer are not TR conjugates of each other, such that this scattering is not protected by TR symmetry. These scattering processes can arise from electromagnetic fields perpendicular to the layer plane or due to out-of-plane acoustic phonons, which enhance the interlayer coupling (see Table II). The availability of acoustic phonons at the Γ point at low temperatures and the presence of environmental charge noise implies that spins in CB2 (CB1) states in W-based (Mo-based) TMDs will suffer from significantly faster relaxation than their counterparts in ML TMDs.

Additional interlayer energy-conserving spin-flipping scattering processes also arise for states transforming as $K_{4,5}$. These processes must be driven by operators transforming as the E IR of the point group C_3, corresponding to electromagnetic fields in the layer plane, and longitudinal and transverse acoustic phonon modes in the Γ point (Table II). Again, these processes are expected to be prevalent even at low temperatures, leading to fast spin relaxation.

Finally, additional interlayer spin-flipping processes that modify the linear momentum of charge carriers, i.e., interlayer intervalley processes [Fig. 3(d)], also arise. Due to requirements of momentum conservation, these processes must be accompanied by the emission or absorption of a K phonon. Since they involve a change in the energy of the charge carriers of at least a few tens of meVs, upward scattering processes (CB1 $\rightarrow$ CB2) are likely suppressed at low temperatures. Relaxation of hot carriers accompanied by a spin flip and change in linear momentum (CB2 $\rightarrow$ CB1), however, may arise via the emission of K phonons transforming as E. Additionally, in-plane momentum transfer from the the CB at the K point of one layer into the VB at the K' point of the other layer [transitions denoted by dashed lines in Fig. 3(d)] are only allowed by second-order processes involving a photon and a phonon, transforming as the IR A of group C_3. Therefore, these transitions should be suppressed at low temperatures.

The considerations in the earlier paragraphs imply that interlayer scattering processes in bilayers (or few-layer stacks) lead to additional spin-relaxation channels, hindering their application in the field of spintronics. However, they also imply that in these materials, we have additional control over spin-flipping processes. Kerr rotation experiments in W-based bulk TMDs show that the spin polarization in these materials decays within tens of ps [39]. Although much shorter than their counterparts in ML samples [18,43,44], these spin lifetimes still enable optical detection with high resolution. The group-theoretical results of this section indicate that externally applied electric fields, for example, could be used to manipulate the spin-scattering rates in these materials, allowing us to turn these optically induced spin signals on/off electrically [38,43]. Furthermore, in-plane and out-of-plane electric field studies could unravel the charge character of the spin polarization. This results from the fact that in-plane electric fields will impact the spin-scattering processes of optically created holes, whereas out-of-plane electric fields will impact the scattering processes of optically created electrons.

Several approaches could be used to enhance the spin lifetimes in bilayer TMDs. On the one hand, we expect that encapsulating bilayer and bulk devices with van der Waals insulators such as hBN will be important in reducing the electrostatic influence of substrate or adsorbed charges. The electrostatic environment of the BL could be further controlled by gating, possibly leading to longer spin lifetimes. On the other hand, heterostructures of TMDs will have different interlayer coupling and interfacial electric dipoles, depending on the particular combination of materials. Engineering these parameters, for example, could significantly suppress interlayer scattering mechanisms, leading to spin lifetimes more similar to those found in ML TMDs [45]. Additionally, the phonon spectra can also be modified by strain or the coupling to other van der Waals materials in heterostructures. In these devices, one could think of deliberately enhancing interlayer scattering processes via applied electric fields, combining the long spin lifetimes observed in ML TMDs with the enhanced electrical control of spin polarization provided by multilayer stacks.

Finally, we note that optical fields, such as circularly polarized light, will couple to a certain spin species according to the selection rules established above. When one applies an additional static electric or magnetic field that induces state mixing between different layers, this picture still does not change, i.e., circularly polarized light will still couple to the same spin species. However, when the optical field is turned off, the spin polarization will evolve according to the coupled Hamiltonian given by the perturbing static electric or magnetic field. This leads to an oscillation between the two states in time, reminiscent of what is observed in experiments studying the coherent evolution of optically created spins in III-V and II-VI semiconductors, for example [46,47]. These (Rabi) oscillations will decay according to the characteristic spin relaxation and dephasing times [38].

IV. CONCLUSION

Group theory is a powerful tool in the analysis of both equilibrium and out-of-equilibrium physical processes in a variety of materials, including TMDs. It allows one to gain insight into complex physical phenomena from a mathematically simple and comprehensive tool, without needing the specifics of the material of interest. Additionally, it allows one to broadly generalize insights obtained for one material or set of electronic eigenstates without additional computational cost. This approach is simplistic and relies on a series of approximations. Nonetheless, we have shown here that it helps to unveil the fundamental processes at play in various experiments on TMDs. Even the behavior of excitons—for which the presence of exchange interaction is not encompassed by the single-particle approach undertaken here—can often be explained qualitatively by this group-theoretical model, by treating the electron and hole separately [19].

Based on this group-theoretical approach, we could identify fundamental symmetry properties of spins in TMDs and the subsequent selection rules for spin-scattering processes. In ML TMDs, charge carriers in each of the subbands of the CB behave in a fundamentally different manner: for one of the CB subbands, energy-conserving spin-flipping processes are forbidden by TR symmetry, suppressing most of the phonon-related spin flips at low temperatures. This is not true for the other subband of the CB, and for the VB, such that charge carriers in these states can have their spin flipped via scattering from a K phonon. Thus, in Mo-based TMDs—where the states that are symmetry protected with regards to spin flips sit at the bottom of the CB and the SOC splitting in the CB is smaller—magnetic impurities should be the main source of spin-flipping scattering at low temperatures. In these materials, the quality of the sample can drastically enhance the spin lifetime of electrons in the edge of the CB, possibly explaining the broad variation of spin lifetimes reported in the literature. Additionally, we find that spin scattering in ML TMDs is very robust with respect to electric fields, with only fields in the optical range actually giving rise to spin flips, and for a restricted set of states. In contrast, in BL TMDs, all electronic states can undergo spin flips after interacting with electric fields that cause interlayer momentum-conserving transitions. Thus, noisy electric fields, an inhomogeneous electrostatic environment, and acoustic phonons are expected to greatly suppress a spin polarization induced in these materials, and decrease their lifetime. Nonetheless, this feature can also be harnessed to gain control over optically created and detected spin polarization in these materials via electrostatic gating, for example. There, one can use an out-of-plane electric field to efficiently control the spin relaxation in these materials, making it a viable option for spin-based information processing.

ACKNOWLEDGMENT

This work was supported by the Zernike Institute for Advanced Materials and the Dutch Research Council (NWO, Grant No. STU.019.014).

[1] D. Xiao, G. B. Liu, W. Feng, X. Xu, and W. Yao, Coupled Spin and Valley Physics in Monolayers of MoS_2 and Other Group-Vi Dichalcogenides, Phys. Rev. Lett. **108**, 196802 (2012).

[2] K. F. Mak, K. He, J. Shan, and T. F. Heinz, Control of valley polarization in monolayer MoS_2 by optical helicity, Nat. Nanotechnol. **7**, 494 (2012).

[3] H. Zeng, J. Dai, W. Yao, D. Xiao, and X. Cui, Valley polarization in MoS_2 monolayers by optical pumping, Nat. Nanotechnol. **7**, 490 (2012).

[4] X. Xu, W. Yao, D. Xiao, and T. F. Heinz, Spin and pseudospins in layered transition metal dichalcogenides, Nat. Phys. **10**, 343 (2014).

[5] G. Wang, A. Chernikov, M. M. Glazov, T. F. Heinz, X. Marie, T. Amand, and B. Urbaszek, Colloquium: Excitons in atomically thin transition metal dichalcogenides, Rev. Mod. Phys. **90**, 021001 (2018).

[6] K. F. Mak and J. Shan, Photonics and optoelectronics of 2D semiconductor transition metal dichalcogenides, Nat. Photon. **10**, 216 (2016).

[7] Y. Liu, N. O. Weiss, X. Duan, H.-C. Cheng, Yu. Huang, and X. Duan, Van der Waals heterostructures and devices, Nat. Rev. Mater. **1**, 16042 (2016).

[8] J. R. Schaibley, H. Yu, G. Clark, P. Rivera, J. S. Ross, K. L. Seyler, W. Yao, and X. Xu, Valleytronics in 2D materials, Nat. Rev. Mater. **1**, 16055 (2016).

[9] D. Zhong, K. L. Seyler, X. Linpeng, R. Cheng, N. Sivadas, B. Huang, E. Schmidgall, T. Taniguchi, K. Watanabe, M. A. McGuire, W. Yao, D. Xiao, K. C. Fu, and X. Xu, Van der Waals engineering of ferromagnetic semiconductor heterostructures for spin and valleytronics, Sci. Adv. **3**, e1603113 (2017).

[10] Y. K. Luo, J. Xu, T. Zhu, G. Wu, E. J. McCormick, W. Zhan, M. R. Neupane, and R. K. Kawakami, Opto-valleytronic spin injection in monolayer MoS_2/few-layer graphene hybrid spin valves, Nano Lett. **17**, 3877 (2017).

[11] A. Avsar, D. Unuchek, J. Liu, O. L. Sanchez, K. Watanabe, T. Taniguchi, B. Ozyilmaz, and A. Kis, Optospintronics in graphene via proximity coupling, ACS Nano **11**, 11678 (2017).

[12] J. Ribeiro-Soares, R. M. Almeida, E. B. Barros, P. T. Araujo, M. S. Dresselhaus, L. G. Cancado, and A. Jorio, Group theory analysis of phonons in two-dimensional transition metal dichalcogenides, Phys. Rev. B **90**, 115438 (2014).

[13] D. Lagarde, L. Bouet, X. Marie, C. R. Zhu, B. L. Liu, T. Amand, P. H. Tan, and B. Urbaszek, Carrier and Polarization Dynamics in Monolayer MoS_2, Phys. Rev. Lett. **112**, 047401 (2014).

[14] C. Mai, Y. G. Semenov, A. Barrette, Y. Yu, Z. Jin, L. Cao, K. W. Kim, and K. Gundogdu, Exciton valley relaxation in a single layer of WS_2 measured by ultrafast spectroscopy, Phys. Rev. B **90**, 041414(R) (2014).

[15] W. T. Hsu, Y. L. Chen, C. H. Chen, P. S. Liu, T. H. Hou, L. J. Li, and W. H. Chang, Optically initialized robust valley-polarized holes in monolayer WSe_2, Nat. Commun. **6**, 8963 (2015).

[16] L. Y. Yang, N. A. Sinitsyn, W. B. Chen, J. T. Yuan, J. Zhang, J. Lou, and S. A. Crooker, Long-lived nanosecond spin relaxation and spin coherence of electrons in monolayer MoS_2 and WS_2, Nat. Phys. **11**, 830 (2015).

[17] M. Ersfeld, F. Volmer, P. de Melo, R. de Winter, M. Heithoff, Z. Zanolli, C. Stampfer, M. J. Verstraete, and B. Beschoten, Spin states protected from intrinsic electron-phonon coupling reaching 100 ns lifetime at room temperature in $MoSe_2$, Nano Lett. **19**, 4083 (2019).

[18] X. Song, S. Xie, K. Kang, J. Park, and V. Sih, Long-lived hole spin/valley polarization probed by Kerr rotation in monolayer WSe_2, Nano Lett. **16**, 5010 (2016).

[19] C. Robert, T. Amand, F. Cadiz, D. Lagarde, E. Courtade, M. Manca, T. Taniguchi, K. Watanabe, B. Urbaszek, and X. Marie, Fine structure and lifetime of dark excitons in transition metal dichalcogenide monolayers, Phys. Rev. B **96**, 155423 (2017).

[20] C. Robert, B. Han, P. Kapuscinski, A. Delhomme, C. Faugeras, T. Amand, M. R. Molas, M. Bartos, K. Watanabe, T. Taniguchi, B. Urbaszek, M. Potemski, and X. Marie, Measurement of the spin-forbidden dark excitons in MoS_2 and $MoSe_2$ monolayers, Nat. Commun. **11**, 4037 (2020).

[21] Y. Song and H. Dery, Transport Theory of Monolayer Transition-Metal Dichalcogenides Through Symmetry, Phys. Rev. Lett. **111**, 026601 (2013).

[22] A. Kormányos, V. Zólyomi, V. I. Fal'ko, and G. Burkard, Tunable Berry curvature and valley and spin Hall effect in bilayer MoS_2, Phys. Rev. B **98**, 035408 (2018).

[23] J. Forste, N. V. Tepliakov, S. Y. Kruchinin, J. Lindlau, V. Funk, M. Forg, K. Watanabe, T. Taniguchi, A. S. Baimuratov, and A. Hogele, Exciton g-factors in monolayer and bilayer WSe_2 from experiment and theory, Nat. Commun. **11**, 4539 (2020).

[24] J. Silva-Guillén, P. San-Jose, and R. Roldán, Electronic band structure of transition metal dichalcogenides from *ab initio* and Slater–Koster tight-binding model, Appl. Sci. **6**, 284 (2016).

[25] A. Kormányos, G. Burkard, M. Gmitra, J. Fabian, V. Zólyomi, N. D. Drummond, and V. Fal'ko, **k·p** theory for two-dimensional transition metal dichalcogenide semiconductors, 2D Mater. **2**, 022001 (2015).

[26] G.-B. Liu, W.-Y. Shan, Y. Yao, W. Yao, and D. Xiao, Three-band tight-binding model for monolayers of group-VIB transition metal dichalcogenides, Phys. Rev. B **88**, 085433 (2013).

[27] M. S. Dresselhaus, G. Dresselhaus, and A. Jorio, *Group Theory* (Springer-Verlag, Berlin, 2008).

[28] C. Jiang, F. Liu, J. Cuadra, Z. Huang, K. Li, A. Rasmita, A. Srivastava, Z. Liu, and W. B. Gao, Zeeman splitting via spin-valley-layer coupling in bilayer $MoTe_2$, Nat. Commun. **8**, 802 (2017).

[29] G. Aivazian, Z. Gong, A. M. Jones, R.-L. Chu, J. Yan, D. G. Mandrus, C. Zhang, D. Cobden, W. Yao, and X. Xu, Magnetic control of valley pseudospin in monolayer WSe_2, Nat. Phys. **11**, 148 (2015).

[30] A. Srivastava, M. Sidler, A. V. Allain, D. S. Lembke, A. Kis, and A. Imamoğlu, Valley zeeman effect in elementary optical excitations of monolayer WSe_2, Nat. Phys. **11**, 141 (2015).

[31] See Supplemental Material at http://link.aps.org/supplemental/10.1103/PhysRevB.103.115410 for character tables of the relevant groups, selection rules at other points of the BZ, and spin-conserving selection rules.

[32] G. Wang, C. Robert, M. M. Glazov, F. Cadiz, E. Courtade, T. Amand, D. Lagarde, T. Taniguchi, K. Watanabe, B. Urbaszek, and X. Marie, In-Plane Propagation of Light in Transition Metal Dichalcogenide Monolayers: Optical Selection Rules, Phys. Rev. Lett. **119**, 047401 (2017).

[33] X. X. Zhang, T. Cao, Z. Lu, Y. C. Lin, F. Zhang, Y. Wang, Z. Li, J. C. Hone, J. A. Robinson, D. Smirnov, S. G. Louie, and T. F. Heinz, Magnetic brightening and control of dark excitons in monolayer WSe_2, Nat. Nanotechnol. **12**, 883 (2017).

[34] X. Zhang, X. F. Qiao, W. Shi, J. B. Wu, D. S. Jiang, and P. H. Tan, Phonon and raman scattering of two-dimensional transition metal dichalcogenides from monolayer, multilayer to bulk material, Chem. Soc. Rev. **44**, 2757 (2015).

[35] L. Zhang and Q. Niu, Chiral Phonons at High-Symmetry Points in Monolayer Hexagonal Lattices, Phys. Rev. Lett. **115**, 115502 (2015).

[36] Y. C. Wu, S. Samudrala, A. McClung, T. Taniguchi, K. Watanabe, A. Arbabi, and J. Yan, Up- and down-conversion between intra- and intervalley excitons in waveguide coupled monolayer WSe_2, ACS Nano **14**, 10503 (2020).

[37] X. W. Zhang, Q. H. Liu, J. W. Luo, A. J. Freeman, and A. Zunger, Hidden spin polarization in inversion-symmetric bulk crystals, Nat. Phys. **10**, 387 (2014).

[38] Z. Gong, G. B. Liu, H. Yu, D. Xiao, X. Cui, X. Xu, and W. Yao, Magnetoelectric effects and valley-controlled spin quantum gates in transition metal dichalcogenide bilayers, Nat. Commun. **4**, 2053 (2013).

[39] M. H. D. Guimaraes and B. Koopmans, Spin Accumulation and Dynamics in Inversion-Symmetric Van Der Waals Crystals, Phys. Rev. Lett. **120**, 266801 (2018).

[40] J. M. Riley, F. Mazzola, M. Dendzik, M. Michiardi, T. Takayama, L. Bawden, C. Granerød, M. Leandersson, T. Balasubramanian, M. Hoesch, T. K. Kim, H. Takagi, W. Meevasana, Ph. Hofmann, M. S. Bahramy, J. W. Wells, and P. D. C. King, Direct observation of spin-polarized bulk bands in an inversion-symmetric semiconductor, Nat. Phys. **10**, 835 (2014).

[41] J. Ye, Y. Li, T. Yan, G. Zhai, and X. Zhang, Ultrafast dynamics of spin generation and relaxation in layered WSe_2, J. Phys. Chem. Lett. **10**, 2963 (2019).

[42] Y. Li, X. Wei, J. Ye, G. Zhai, K. Wang, and X. Zhang, Gate-controlled spin relaxation in bulk WSe_2 flakes, AIP Adv. **10**, 045315 (2020).

[43] A. M. Jones, H. Y. Yu, J. S. Ross, P. Klement, N. J. Ghimire, J. Q. Yan, D. G. Mandrus, W. Yao, and X. D. Xu, Spin-layer locking effects in optical orientation of exciton spin in bilayer WSe_2, Nat. Phys. **10**, 130 (2014).

[44] F. Volmer, S. Pissinger, M. Ersfeld, S. Kuhlen, C. Stampfer, and B. Beschoten, Intervalley dark trion states with spin lifetimes of 150 ns in WSe_2, Phys. Rev. B **95**, 235408 (2017).

[45] P. Rivera, H. Yu, K. L. Seyler, N. P. Wilson, W. Yao, and X. Xu, Interlayer valley excitons in heterobilayers of transition metal dichalcogenides, Nat. Nanotechnol. **13**, 1004 (2018).

[46] J. M. Kikkawa, I. P. Smorchkova, N. Samarth, and D. D. Awschalom, Room-temperature spin memory in two-dimensional electron gases, Science **277**, 1284 (1997).

[47] A. V. Kimel, F. Bentivegna, V. N. Gridnev, V. V. Pavlov, R. V. Pisarev, and Th. Rasing, Room-temperature ultrafast carrier and spin dynamics in GaAs probed by the photoinduced magneto-optical Kerr effect, Phys. Rev. B **63**, 235201 (2001).